Chem Biol Drug Des 2012; **79:** 897–906

Research Article

doi: 10.1111/j.1747-0285.2012.01365.x

Synthesis, Structure–Activity Relationship, and Pharmacophore Modeling Studies of Pyrazole-3-Carbohydrazone Derivatives as Dipeptidyl Peptidase IV Inhibitors

Deyan Wu[1,†], Fangfang Jin[1,†], Weiqiang Lu[1,†], Jin Zhu[1], Cui Li[1], Wei Wang[1], Yun Tang[1], Hualiang Jiang[1,2], Jin Huang[1,*], Guixia Liu[1,*] and Jian Li[1,*]

[1]*Shanghai Key Laboratory of New Drug Design, School of Pharmacy, East China University of Science and Technology, 130 Mei Long Road, Shanghai 200237, China*

[2]*Drug Discovery and Design Center, Shanghai Institute of Materia Medica, Chinese Academy of Sciences, 555 Zu Chong Zhi Road, Shanghai 201203, China*

**Corresponding authors: Jin Huang, huangjin@ecust.edu.cn; Guixia Liu, gxliu@ecust.edu.cn; Jian Li, jianli@ecust.edu.cn*

[†]*These authors contributed equally to this work.*

Type 2 diabetes mellitus (T2DM) is a metabolic disease and a major challenge to healthcare systems around the world. Dipeptidyl peptidase IV (DPP-4), a serine protease, has been rapidly emerging as an effective therapeutic target for the treatment for T2DM. In this study, a series of novel DPP-4 inhibitors, featuring the pyrazole-3-carbohydrazone scaffold, have been discovered using an integrated approach of structure-based virtual screening, chemical synthesis, and bioassay. Virtual screening of SPECS Database, followed by enzymatic activity assay, resulted in five micromolar or low-to-mid-micromolar inhibitory level compounds (1–5) with different scaffold. Compound 1 was selected for the further structure modifications in considering inhibitory activity, structural variability, and synthetic accessibility. Seventeen new compounds were synthesized and tested with biological assays. Nine compounds (6e, 6g, 6k–l, and 7a–e) were found to show inhibitory effects against DPP-4. Molecular docking models give rational explanation about structure–activity relationships. Based on eight DPP-4 inhibitors (1–5, 6e, 6k, and 7d), the best pharmacophore model hypo1 was obtained, consisting of one hydrogen bond donor (HBD), one hydrogen bond acceptor (HBA), and two hydrophobic (HY) features. Both docking models and pharmacophore mapping results are in agreement with pharmacological results. The present studies give some guiding information for further structural optimization and are helpful for future DPP-4 inhibitors design.

Key words: dipeptidyl peptidase IV, inhibitors, molecular docking, pharmacophore modeling, synthesis

Received 19 October 2011, revised 11 January 2012 and accepted for publication 17 February 2012

Type 2 diabetes mellitus (T2DM) is a metabolic disease and has become a worldwide epidemic. Currently, approximate 194 million people in worldwide are affected by this disease and this number is forecasted to increase to 366 million by 2030[a',b]. The health, social, and economic burden of T2DM is significant; consequently, T2DM presents a major challenge to healthcare systems around the world.[c]

The current oral treatment options for T2DM include metformin, sulfonylurea (SU) or thiazolidinedione (TZD) derivatives, glycosidase inhibitors, and the recently introduced dipeptidyl peptidase IV (DPP-4) inhibitors. DPP-4 is a serine protease that is ubiquitously expressed as both a membrane-bound protein and a soluble protein in plasma (1,2). It mediates the activities of regulatory peptides by cleaving dipeptides from the N-terminus of glucagon-like peptide-1 amide (GLP-1-NH2) and glucose-dependent insulinotropic polypeptide (GIP) to yield inactive GLP-1-NH2 peptide and GIP, respectively (3,4). Consequently, inhibition of DPP-4 is rapidly emerging as a novel therapeutic approach for the treatment for type 2 diabetes. To data, a large number of DPP-4 inhibitors have been reported in the literature. Among them, MK-0431 (Sitagliptin) (5), which is the first approved DPP-4 inhibitor, has been prescribed in the United States since 2006. LAF-237 (Vildagliptin) (6) was approved in Europe in 2007, and BMS-477118 (Saxagliptin) (7) has been approved and on the market in the United States in 2009. SYR-322 (Alogliptin) (8) was approved in Japan in 2010, and BI-1356 (Linagliptin) (9) was approved by the US FAD in May 2011.

With the aim to find new scaffold inhibitors of DPP-4, structure-based virtual screening had been employed in our laboratory to screen the SPECS Database against the crystal structure of DPP-4 (PDB code: 2P8S) (10). And five micromolar or low-to-mid-micromolar inhibitory level compounds (**1**–**5**) with different scaffold were successfully identified (Figure 1) after bioassay verification. Considering inhibitory activity, structural variability, and synthetic accessibility of compound **1**, it may serve as a reasonable lead compound for the further structure modifications. To provide expedient and significant structure–activity relationship (SAR) information and improve inhibitory activity of the lead compound **1**, chemical

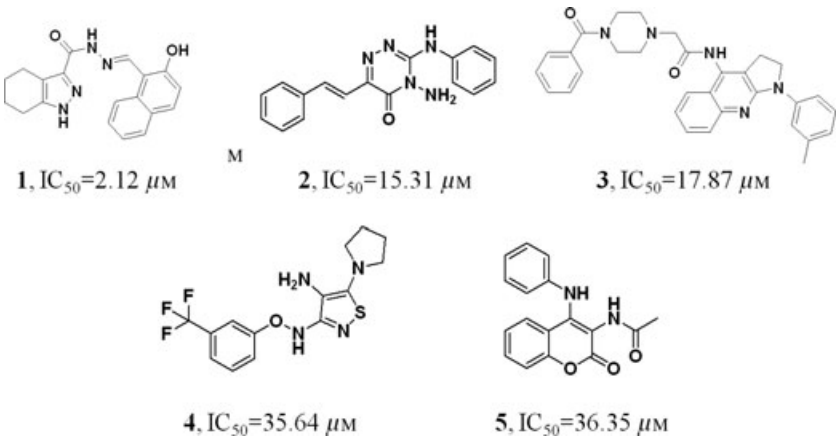

Figure 1: The structures and their DPP-4 inhibitory activities of compounds **1**–**5** selected from the candidates by virtual screening and bioassay.

modifications were performed in two cycles, by maintaining the pyrazole-3-carbohydrazone scaffold. Totally, seventeen analogs (**6a**–**l** and **7a**–**e**) of compound **1** have been synthesized and tested against DPP-4. Finally, nine compounds (**6e**, **6g**, **6k**–**l,** and **7a**–**e**) were found to show micromolar or low-to-mid-micromolar level inhibitory effects against DPP-4, generally 2–35 times lower than the lead compound **1**. To reasonably explain the activity loss of compounds **6**–**7**, subsequently, the SARs of the pyrazole-3-carbohydrazone scaffold (**1** and **6**–**7**) were summarized tentatively; the binding modes of inhibitors **6k** and **7c** to DPP-4 were compared with that of inhibitor **1** by means of the molecular docking; eight compounds (**1**–**5**, **6e**, **6k**, and **7d**) were employed to generate the pharmacophore model of DPP-4 inhibitors. These results give some guiding information for further structural optimization and are helpful for future DPP-4 inhibitors design.

Experimental Section

Computational modeling

Molecular docking

Docking experiments were performed using GLIDE 5.0 included in SCHRÖDINGER Package, MASTRO INTERFACE version 9.0.[d] The co-ordinates for the X-ray crystal structure of DPP-4 (PDB code: 2P8S) (10) was obtained from the RCSB Protein Data Bank. Before the molecular docking process, the ligand of the crystal structure was removed and then the free protein was modified by adding hydrogen atoms using the protein preparation workflow. Molecules to be docked were prepared and energy-minimized according to standard procedure of LigPrep module implemented in MAESTRO 9.0.[e]

In the molecular docking process, standard-precision (SP) docking method was adopted to generate the minimized pose, and the Glide scoring function (GIide Score) was used to select the final poses for each ligand.

Ligand-based pharmacophore modeling

Common feature pharmacophore hypotheses were generated using the HipHopRefine algorithm based on eight DPP-4 inhibitors (**1**–**5**, **6e**, **6k**, and **7d**). The structures and conformations of the eight compounds were built within Catalyst (Accelrys Inc.).[f] Compound **1** was considered as the reference compound specifying a Principal value of 2 and a MaxOmitFeat value of 0, meaning its structure and conformation would have the strongest influence on the model building phase. The Principal value and MaxOmitFeat value for the remaining compounds were set to 1 and 1, respectively. The Poling algorithm implemented within Catalyst was used to generate conformations for all of the compounds. For each compound, possible diverse sets of conformations were generated over a 20 kcal/mol range using the BEST flexible conformation generation option available in Catalyst. The chemical features considered in the pharmacophore model generation run were H-bond acceptor (HBA), H-bond donor (HBD), hydrophobic (HY), and positively ionizable (PI) features. HipHop was set to consider these features in the generation of the pharmacophore hypotheses.

Synthesis

General methods

Anhydrous ethyl alcohol was dried by distillation from calcium hydride. Other solvents and commercial chemicals were purchased at the highest commercial quality and we reused without further purification, unless otherwise indicated. Reactions requiring anhydrous conditions were performed under nitrogen or a calcium chloride tube. Melting points were determined on a SGW X-4 melting point apparatus without correction. Nuclear magnetic resonance (NMR) spectroscopy was obtained on a Bruker-400, in $CDCl_3$ or DMSO-d_6 solutions, and chemical shifts were measured in ppm downfield from an internal tetramethylsilane (TMS) standard. The following abbreviations are used: s (singlet), d (doublet), t (triplet), q (quartet), bs (broad singlet), m (multiplet), etc. Coupling constants were reported in Hz. Low- and high-resolution mass spectra (LRMS and HRMS) were given with electric and matrix-assisted laser desorption ionization (EI and MALDI) produced by Finnigan MAT-95 and IonSpec 4.7 T. The products were purified by recrystallization or column chromatography on silica gel (200–300 mesh). Thin-layer chromatography (TLC) was carried out with HSGF 254 (150–200 μm thickness; Yantai Huiyou Co., China), and components were visualized by observation under UV light (254 and 365 nm).

*Ethyl 2-oxo-2-(2-oxocyclohexyl)acetate (**9a**)*: A solution of Sodium ethoxide was prepared by the cautious addition of 2.55 g

(110 mmol) of sodium to 40 mL of anhydrous ethyl alcohol in a 250 mL three-necked flask equipped with a dropping funnel, and a reflux condenser carrying a calcium chloride tube. The flask was then immersed in an ice bath and the stirrer was started. Then, a cold solution of 10.5 mL (100 mmol) of cyclohexanone in 13.5 mL (100 mmol) of ethyl oxalate was added from the dropping funnel over a period of about 15 min. When the addition was complete, the ice bath was retained for 1 h, and then the mixture was stirred at room temperature for another 6 h (11). The reaction mixture was added to ice water and acidified by the addition of 2 N HCl. The aqueous solution was extracted with CH_2Cl_2 (3 × 40 mL), washed with brine, dried over anhydrous $MgSO_4$, and evaporated to give the residue, which was purified by flash column chromatography on silica gel, eluted with a mixture of EtOAc/petroleum ether (1:25, v/v), to afford **9a** (11.5 g, 59%) as a solid. ^{1}HNMR (400 MHz, $CDCl_3$) δ 6.27 (s, 1H), 5.32 (t, J = 4.8 Hz, 1H), 3.77 (q, J = 7.2 Hz, 2H), 3.00 (t, J = 5.6 Hz, 2H), 2.26 (q, J = 5.6 Hz, 2H), 1.68 (m, 2H), 1.34 (t, J = 7.2 Hz, 3H).

*Ethyl 4,5,6,7-tetrahydro-1H-indazole-3-carboxylate(**10a**)*: Ten grams (50.45 mmol) **9a** was dissolved in 20 mL of acetic acid at 0 °C. A total of 3.2 mL (56.50 mmol) of 85% hydrazine hydrate was slowly added. The mixture was heated to reflux for 10 h. After cooling of the sample, the solid matter was filtered and dried in vacuo, resulting in **10a** (9.6 g, 98%) of white crystals (12); ^{1}HNMR (400 MHz, $CDCl_3$) δ 4.38 (q, J = 7.2 Hz, 2H), 2.76 (t, J = 6.0 Hz, 2H), 2.70 (t, J = 6.0 Hz, 2H), 1.84–1.75 (m, 4H), 1.39 (t, J = 7.2 Hz, 3H).

*4,5,6,7-Tetrahydro-1H-indazole-3-carbohydrazide (**11a**)*: A mixture of 5.0 g (25.7 mmol) **10a** and 24.0 mL (350 mmol) of 85% hydrazine hydrate in 100 mL of ethanol was refluxed for 36 h then cooled. The solid collected by filtration, washed with water, and dried in vacuo, gave **11a** (4.6 g, 100%) (13); ^{1}HNMR (400 MHz, DMSO-d_6) δ 2.74 (t, J = 5.6 Hz, 2H), 2.66 (t, J = 5.6 Hz, 2H), 1.83–1.77 (m, 4H).

*N′-[(2-Hydroxy-naphthalen-1-yl)methylene]-4,5,6,7-tetrahydro-1H-indazole-3-carbohydrazone (**1**)*: A mixture of **11a** (180 mg, 1 mmol), 2-Hydroxy-1-naphthaldehyde (190 mg, 1.1 mmol),and acetic acid (20 μL) in 5 mL of ethanol was refluxed for 6 h, then cooled. The solid collected by filtration, washed with ethanol, and dried in vacuo, gave **1** (318 mg, 95%); mp = 298–317 °C; ^{1}HNMR (400 MHz, DMSO-d_6) δ 13.05 (s, 1H), 12.98 (s, 1H), 11.97 (s, 1H), 9.66 (s, 1H), 8.12 (d, J = 8.4 Hz, 1H), 7.91 (t, J = 7.2 Hz, 2H), 7.60 (t, J = 7.6 Hz, 1H), 7.41 (t, J = 7.2 Hz, 1H), 7.22 (d, J = 8.8 Hz, 1H), 2.72 (t, J = 5.2 Hz, 2H), 2.65 (t, J = 5.6 Hz, 2H), 1.77–1.71 (m, 4H); EI-MS m/z 334.1 (M^+), 149.1 (100%); HRMS (EI) m/z calcd $C_{19}H_{18}N_4O_2$ (M^+) 334.1430, found 334.1436.

*N′-[(2-Hydroxy-phenyl)methylene]-4,5,6,7-tetrahydro-1H-indazole-3-carbohydrazone (**6a**)*: Starting with **11a** and 2-Hydroxybenzaldehyde, the same procedures were followed as in the synthesis of **1**. Yield = 48%; mp = 280–287 °C; ^{1}HNMR (400 MHz, DMSO-d_6) δ 12.99 (s, 1H), 11.92 (s, 1H), 11.54 (s, 1H), 8.66 (s, 1H), 7.39 (d, J = 7.6 Hz, 1H), 7.29 (t, J = 8.8 Hz, 1H), 6.94 (d, J = 7.6 Hz, 1H), 6.90 (t, J = 7.2 Hz, 1H), 2.69 (t, J = 5.6 Hz, 2H), 2.63 (t, J = 6.0 Hz, 2H), 1.76–1.69 (m, 4H); EI-MS m/z 284.1 (M^+), 149.1 (100%); HRMS (EI) m/z calcd $C_{15}H_{16}N_4O_2$ (M^+) 284.1273; found 284.1272.

N′-[(4-Cyano-phenyl)methylene]-4,5,6,7-tetrahydro-1H-indazole-3-carbohydrazone (6b): Starting with **11a** and 4-cyanobenzaldehyde, the same procedures were followed as in the synthesis of **1**. Yield = 84%; mp = 314–328 °C; ^{1}HNMR (400 MHz, DMSO-d_6) δ 12.98 (s, 1 H), 11.80 (s, 1H), 8.55 (s, 1H), 7.90 (d, J = 8.4 Hz, 2H), 7.83 (d, J = 8.4 Hz, 2H), 2.69 (t, J = 6.0 Hz, 2H), 2.63 (t, J = 6.0 Hz, 2H), 1.75–1.69 (m, 4H); EI-MS m/z 293.1 (M^+), 149.1 (100%); HRMS (EI) m/z calcd $C_{16}H_{15}N_5O$ (M^+) 293.1277; found 293.1278.

*N′-[(4-Chloro-3-fluorophenyl)methylene]-4,5,6,7-tetrahydro-1H-indazole-3-carbohydrazone(**6c**)*: Starting with **11a** and 4-chloro-3-fluorobenzaldehyde, the same procedures were followed as in the synthesis of **1**. Yield = 80%; mp = 311–315 °C; ^{1}HNMR (400 MHz, DMSO-d_6) δ 12.96 (s, 1H), 11.73 (s, 1H), 8.45 (s, 1H), 7.66 (m, 2H), 7.52 (d, J = 8.4 Hz, 1H), 2.68 (t, J = 6.0 Hz, 2H), 2.63 (t, J = 6.0 Hz, 2H), 1.75–1.68 (m, 4H); EI-MS m/z 320.1 (M^+), 149.1 (100%); HRMS (EI) m/z calcd $C_{15}H_{14}ClFN_4O$ (M^+) 320.0840; found 320.0844.

*N′-[(4-Chloro-3-nitrophenyl)methylene]-4,5,6,7-tetrahydro-1H-indazole-3-carbohydrazone (**6d**)*: Starting with **11a** and 4-chloro-3-nitrobenzaldehyde, the same procedures were followed as in the synthesis of **1**. Yield = 65%; mp = 299–302 °C; 1HNMR (400 MHz, DMSO-d_6) δ 13.00 (s, 1H), 11.89 (s, 1H), 8.55 (s, 1H), 8.31 (s, 1H), 7.97 (d, J = 8.4Hz, 1H), 7.84 (d, J = 8.4 Hz, 1H), 2.68 (t, J = 5.6 Hz, 2H), 2.63 (t, J = 6.0 Hz, 2H), 1.76–1.69 (m, 4H); EI-MS m/z 347.1 (M^+), 149.1 (100%); HRMS (EI) m/z calcd $C_{15}H_{14}ClN_5O_3$ (M^+) 347.0785; found 347.0786.

*N′-[1-(2,4-Dihydroxyphenyl)ethylidene]-4,5,6,7-tetrahydro-1H-indazole-3-carbohydrazone (**6e**)*: A mixture of **11a** (180 mg, 1 mmol), 2,4-dihydroxyacetophenone (167 mg, 1.1 mmol), and acetic acid (20 μL) in 5 mL of ethanol was refluxed for 16 h then cooled. The solid collected by filtration, washed with ethanol, and dried in vacuo, gave **6e** (85 mg, 27%); mp = 292–304 °C; ^{1}HNMR (400 MHz, DMSO-d_6) δ 13.44 (s, 1H), 12.97 (s, 1H), 10.58 (s, 1H), 9.56 (s, 1H), 7.43 (d, J = 8.8 Hz, 1H), 6.32 (d, J = 8.8 Hz, 1H), 6.27 (s, 1H), 2.69 (t, J = 5.2 Hz, 2H), 2.62 (t, J = 5.6 Hz, 2H), 2.35 (s, 3H), 1.75–1.64 (m, 4H); EI-MS m/z 314.1 (M^+), 149.1 (100%); HRMS (EI) m/z calcd $C_{16}H_{18}N_4O_3$ (M^+) 314.1379; found 314.1380.

*N′-[3,4-Dihydro-1(2H)-naphthalen-1-yl]-4,5,6,7-tetrahydro-1H-indazole-3-carbohydrazone (**6f**)*: Starting with **11a** and 3,4-dihydro-1(2H)-naphthalenone, the same procedures were followed as in the synthesis of **6e**. Yield = 64%; mp = 269–274 °C; ^{1}HNMR (400 MHz, DMSO-d_6) δ 12.93 (s, 1H), 10.12 (s, 1H), 8.05 (d, J = 7.2 Hz, 1H), 7.31 (t, J = 7.2 Hz, 1H), 7.27 (t, J = 7.6 Hz, 1H), 7.21 (d, J = 7.6 Hz, 1H), 2.77(t, J = 6.0 Hz, 2H), 2.74–2.69 (m, 4H), 2.68 (s, 3H), 2.64 (t, J = 5.6 Hz, 2H), 1.91–1.84 (m, 2H), 1.76–1.69 (m, 4H); EI-MS m/z 308.1 (M^+), 149.1 (100%); HRMS (EI) m/z calcd $C_{19}H_{18}ClN_5O$ (M^+) 308.1637; found 308.1636.

*N′-[(1-methyl-1H-pyrrol-2-yl)methylene]-4,5,6,7-tetrahydro-1H-indazole-3-carbohydrazone (**6g**)*: Starting with **11a** and *N*-methylpyrrole-2-carboxaldehyde, the same procedures were followed as in the synthesis of **1**. Yield = 73%; ^{1}HNMR (400 MHz, DMSO-d_6) δ 12.86 (s, 1H), 11.17 (s, 1H), 8.42 (s, 1H), 6.92 (s, 1H), 6.42 (s, 1H), 6.08 (s, 1H), 3.83 (s, 3H), 2.67 (t, J = 6.0 Hz, 2H), 2.60 (t, J = 6.0 Hz, 2H),

1.78–1.69 (m, 4H); EI-MS m/z 271 (M^+), 149 (100%); HRMS (EI) m/z calcd $C_{14}H_{17}N_5O$ (M^+) 271.1433; found 271.1433.

*N'-[(2,4-dihydroxyphenyl)methylene]-4,5,6,7-tetrahydro-1H-indazole-3-carbohydrazone (**6h**)*: Starting with **11a** and 3,4-dihydroxybenzaldehyde, the same procedures were followed as in the synthesis of **1**. Yield = 73%; mp = 268–272 °C; ^{1}HNMR (400 MHz, DMSO-d_6) δ 12.87 (s, 1H), 11.23 (s, 1H), 9.32 (s, 1H), 9.24 (s, 1H), 8.29 (s, 1H), 7.19 (s, 1H), 6.86 (d, J = 8.4 Hz, 1H), 6.76 (d, J = 8.4 Hz, 1H), 2.66 (t, J = 5.6 Hz, 2H), 2.62 (t, J = 6.0 Hz, 2H), 2.35 (s, 3H), 1.75–1.68 (m, 4H); EI-MS m/z 300.1 (M^+), 149.1 (100%); HRMS (EI) m/z calcd $C_{15}H_{16}N_4O_3$ (M^+) 300.1222; found 300.1224.

*N'-cycloheptylidene-4,5,6,7-tetrahydro-1H-indazole-3-carbohydrazone (**6i**)*: Starting with **11a** and cycloheptanone, the same procedures were followed as in the synthesis of **6e**. Yield = 83%; mp = 258–264 °C; ^{1}HNMR (400 MHz, DMSO-d_6) δ 12.83 (s, 1H), 9.68 (s, 1H), 2.67–2.56 (m, 4H), 2.47–2.45 (m, 4H), 1.73–1.67 (m, 6H), 1.60–1.54 (m, 6H); EI-MS m/z 274.2 (M^+), 149.1 (100%); HRMS (EI) m/z calcd $C_{15}H_{22}N_4O$ (M^+) 274.1794; found 274.1792.

*N'-[(3-Chloro-4-hydroxy-5-methoxyphenyl)methylene]-4,5,6,7-tetrahydro-1H-indazole-3-carbohydrazone (**6j**)*: Starting with **11a** and 3-chloro-4-hydroxy-5-methoxy-benzaldehyde, the same procedures were followed as in the synthesis of **1**. Yield = 82%; mp = 313–316 °C; ^{1}HNMR (400 MHz, DMSO-d_6) δ 12.91 (s, 1H), 11.47 (s, 1H), 9.91 (s, 1H), 8.35 (s, 1H), 7.24 (s, 1H), 7.21 (s, 1H), 3.90 (s, 3H), 2.68 (t, J = 4.8 Hz, 2H), 2.63 (t, J = 5.6 Hz, 2H), 1.75–1.68 (m, 4H); EI-MS m/z 348.1 (M^+), 149.1 (100%); HRMS (EI) m/z calcd $C_{16}H_{17}ClN_4O_3$ (M^+) 348.0989; found 348.0990.

*N'-[(Naphthalen-1-yl)methylene]-4,5,6,7-tetrahydro-1H-indazole-3-carbohydrazone (**6k**)*: Starting with **11a** and 1-naphthaldehyde, the same procedures were followed as in the synthesis of **1**. Yield = 90%; mp = 289–293 °C; ^{1}HNMR (400 MHz, DMSO-d_6) δ 12.98 (s, 1H), 11.61 (s, 1H), 9.23 (s, 1H), 8.42 (d, J = 8.4 Hz, 1H), 8.00 (d, J = 8.4 Hz, 2H), 7.91 (d, J = 7.2 Hz, 1H), 7.65 (t, J = 7.2 Hz, 1H), 7.61 (t, J = 7.6 Hz, 2H), 2.73 (t, J = 5.2 Hz, 2H), 2.65 (t, J = 5.6 Hz, 2H), 1.77–1.71 (m, 4H); EI-MS m/z 318.1 (M^+), 149.1 (100%); HRMS (EI) m/z calcd $C_{19}H_{18}N_4O$ (M^+) 318.1481; found 318.1480.

*N'-[(4-Methoxy-naphthalen-1-yl)methylene]-4,5,6,7-tetrahydro-1H-indazole-3-carbohydrazone (**6l**)*: Starting with **11a** and 4-methoxy-1-naphthaldehyde, the same procedures were followed as in the synthesis of **1**. Yield = 92%; mp = 262–265 °C; ^{1}HNMR (400 MHz, DMSO-d_6) δ 12.94 (s, 1H), 11.44 (s, 1H), 9.07 (s, 1H), 8.93 (d, J = 8.4 Hz, 1H), 8.25 (d, J = 8.4 Hz, 1H), 7.82 (d, J = 8.4 Hz, 1H), 7.68 (t, J = 7.6 Hz, 1H), 7.59 (t, J = 7.6 Hz, 1H), 7.10 (d, J = 8.4 Hz, 1H), 4.05 (s, 3H), 2.72 (t, J = 5.2 Hz, 2H), 2.65 (t, J = 5.6 Hz, 2H), 1.78–1.71 (m, 4H); EI-MS m/z 348.1 (M^+), 183.1 (100%); HRMS (EI) m/z calcd $C_{20}H_{20}N_4O_2$ (M^+) 348.1586; found 348.1583.

*Ethyl 2-oxo-2-(2-oxocyclopentyl)acetate (**9b**)*: Starting with cyclopentanone and ethyl oxalate, the same procedures were followed as in the synthesis of **9a**. Yield = 64%; ^{1}HNMR (400 MHz, $CDCl_3$) δ 4.35 (q, J = 7.2 Hz, 2H), 2.96 (t, J = 7.2 Hz, 2H), 2.48 (t, J = 8.0 Hz, 2H), 2.03–1.95 (m, 2H), 1.37 (t, J = 7.2 Hz, 3H).

*Ethyl 1,4,5,6-tetrahydro-cyclopenta[c]pyrazole-3-carboxylate (**10b**)*: Starting with **9b**, the same procedures were followed as in the synthesis of **10a**. Yield = 33%; ^{1}HNMR (400 MHz, $CDCl_3$) δ 4.38 (q, J = 7.2 Hz, 2H), 2.85–2.77 (m, 4H), 2.54–2.46 (m, 2H), 1.40 (t, J = 7.2 Hz, 3H).

*1,4,5,6-Tetrahydro-cyclopenta[c]pyrazole-3-carbohydrazide (**11b**)*: Starting with **10b**, the same procedures were followed as in the synthesis of **11a**. Yield = 53%; ^{1}HNMR (400 MHz, DMSO-d_6) δ 8.97 (s, 1H), 4.38 (bs, 2H), 2.68–2.61 (m, 4H), 2.42–2.38 (m, 2H).

N'-[(2-Hydroxy-naphthalen-1-yl)methylene]-1,4,5,6-tetrahydro-cyclopenta[c]pyrazole-3- carbohydrazone (**7a**): Starting with **11b** and 2-hydroxy-1-naphthaldehyde, the same procedures were followed as in the synthesis of **1**. Yield = 78%; mp = 287–298 °C; ^{1}HNMR (400 MHz, DMSO-d_6) δ 13.08 (s, 1H), 12.94 (s, 1H), 11.96 (s, 1H), 9.64 (s, 1H), 8.13 (d, J = 8.0 Hz, 1H), 7.91 (t, J = 9.2 Hz, 2H), 7.60 (t, J = 7.6 Hz, 1H), 7.41 (t, J = 7.6 Hz, 1H), 7.21 (d, J = 9.2 Hz, 1H), 2.74–2.66 (m, 4H), 2.53–2.49 (m, 2H); EI-MS m/z 320.1 (M^+), 135.1 (100%); HRMS (EI) m/z calcd $C_{18}H_{16}N_4O_2$ (M^+) 320.1273; found 320.1271.

*Ethyl 2-oxo-2-(2-oxocycloheptyl)acetate (**9c**)*: Starting with cycloheptanone and ethyl oxalate, the same procedures were followed as in the synthesis of **9a**. Yield = 87%; ^{1}HNMR (400 MHz, $CDCl_3$) δ 15.50 (s, 1H), 4.35 (q, J = 7.2 Hz, 2H), 2.65 (t, J = 6.4 Hz, 2H), 2.51–2.48 (m, 2H), 1.79–1.63 (m, 6H), 1.37 (t, J = 7.2 Hz, 3H).

*Ethyl 1,4,5,6,7,8-hexahydro-cyclohepta[c]pyrazole-3-carboxylate (**10c**)*: Starting with **9c**, the same procedures were followed as in the synthesis of **10a**. Yield = 88%; ^{1}HNMR (400 MHz, $CDCl_3$) δ 8.37 (s, 1H), 4.38 (q, J = 7.2 Hz, 2H), 2.95 (t, J = 5.6 Hz, 2H), 2.82 (t, J = 5.6 Hz, 2H), 1.90–1.84 (m, 2H), 1.72–1.65 (m, 4H), 1.40 (t, J = 7.2 Hz, 3H).

*1,4,5,6,7,8-Hexahydro-cyclohepta[c]pyrazole-3-carbohydrazide (**11c**)*: Starting with **10c**, the same procedures were followed as in the synthesis of **11a**. Yield = 57%; ^{1}HNMR (400 MHz, DMSO-d_6) δ 8.96 (s, 1H), 4.28 (bs, 2H), 2.84 (s, 2H), 2.67 (t, J = 5.6 Hz, 2H), 1.75 (t, J = 5.2 Hz, 2H), 1.59–1.52 (m, 4H).

*N'-[(2-Hydroxy-naphthalen-1-yl)methylene]-1,4,5,6,7,8-hexahydro-cyclohepta[c]pyrazole-3- carbohydrazone (**7b**)*: Starting with **11c** and 2-hydroxy-1-naphthaldehyde, the same procedures were followed as in the synthesis of **1**. Yield = 86%; mp = 321–327 °C; ^{1}HNMR (400 MHz, DMSO-d_6) δ 13.00 (s, 1H), 12.98 (s, 1H), 11.93 (s, 1H), 9.65 (s, 1H), 8.12 (d, J = 8.8 Hz, 1H), 7.91 (t, J = 8.0 Hz, 2H), 7.60 (t, J = 7.2 Hz, 1H), 7.41 (t, J = 7.2 Hz, 1H), 7.22 (d, J = 8.8 Hz, 1H), 2.99 (t, J = 5.2 Hz, 2H), 2.77 (t, J = 5.6 Hz, 2H), 1.85–1.75 (m, 2H), 1.66–1.61(m, 4H); EI-MS m/z 348.1 (M^+), 163.1 (100%); HRMS (EI) m/z calcd $C_{20}H_{20}N_4O_2$ (M^+) 348.1586; found 348.1588.

*5-(3-Methoxyphenyl)-1H-pyrazole-3-carbohydrazide (**11d**)*: Starting with 3-methoxyacetophenone and ethyl oxalate, the same procedures were followed as in the synthesis of **11a**. Yield = 60%; ^{1}HNMR (400 MHz, DMSO-d_6) δ 13.63 (s, 1H), 9.41 (s, 1H), 7.38–7.34 (m, 3H), 7.14 (s, 1H), 6.91 (d, J = 7.2 Hz, 1H), 4.50 (bs, 2H), 3.81 (s, 3H).

*N'-[(2-Hydroxy-naphthalen-1-yl)methylene]-5-(3-methoxyphenyl)-1H-pyrazole-3-carbohydrazone (**7c**)*: Starting with **11d** and 2-hydroxy-1-naphthaldehyde, the same procedures were followed as in the synthesis of **1**. Yield = 85%; mp = 283–286 °C; ^{1}HNMR (400 MHz, DMSO-d_6) δ 13.88 (s, 1H), 12.93 (s, 1H), 12.15 (s, 1H), 9.69 (s, 1H), 8.18 (d, J = 8.4 Hz, 1H), 7.95 (d, J = 8.8 Hz, 1H), 7.92 (d, J = 8.4 Hz, 1H), 7.62 (t, J = 7.6 Hz, 1H), 7.47–7.40 (m, 4H), 7.31 (s, 1H), 7.25 (d, J = 9.2 Hz, 1H), 7.00 (d, J = 7.6 Hz, 1H), 3.85 (s, 3H); MALDI-MS m/z 387.1 $[M + H]^+$; HRMS (MALDI) m/z calcd $C_{22}H_{19}N_4O_3$ $[M + H]^+$ 387.1457, found 387.1442.

*5-(3-Nitrophenyl)-1H-pyrazole-3-carbohydrazide (**11e**)*: Starting with 3-nitroacetophenone and ethyl oxalate, the same procedures were followed as in the synthesis of **11a**. Yield = 59%; ^{1}HNMR (400 MHz, DMSO-d_6) δ 13.93 (s, 1H), 9.84 (s, 1H), 8.53 (s, 1H), 8.20 (d, J = 7.2 Hz, 2H), 7.75 (t, J = 8.0 Hz, 1H), 7.37 (s, 1H), 4.55 (bs, 2H).

*N'-[(2-Hydroxy-naphthalen-1-yl)methylene]-5-(3-nitrophenyl)-1H-pyrazole-3-carbohydrazone (**7d**)*: Starting with **11e** and 2-hydroxy-1-naphthaldehyde, the same procedures were followed as in the synthesis of **1**. Yield = 69%; mp >300 °C; ^{1}HNMR (400 MHz, DMSO-d_6) δ 14.20 (s, 1H), 12.90 (s, 1H), 12.23 (s, 1H), 9.69 (s, 1H), 8.78 (s, 1H), 8.36 (d, J = 6.8 Hz, 1H), 8.26 (d, J = 8.4 Hz, 1H), 8.18 (d, J = 7.6 Hz, 1H), 7.95 (d, J = 8.8 Hz, 1H), 7.91 (d, J = 8.4 Hz, 1H), 7.80 (t, J = 8.0 Hz, 1H), 7.62 (t, J = 8.0 Hz, 1H), 7.52 (s, 1H),7.42 (t, J = 7.2Hz, 1H); MALDI-MS m/z 402.1 $[M + H]^+$; HRMS (MALDI) m/z calcd $C_{21}H_{16}N_5O_4$ $[M + H]^+$ 402.1202, found 402.1192.

5-(4-Chlorophenyl)-1H-pyrazole-3-carbohydrazide (11f): Starting with 4-chloroacetophenone and ethyl oxalate, the same procedures were followed as in the synthesis of **11a**. Yield = 100%; ^{1}HNMR (400 MHz, DMSO-d_6) δ 7.79 (d, J = 8.4 Hz, 2H), 7.51 (d, J = 8.8 Hz, 2H), 7.15 (s, 1H).

*N'-[(2-Hydroxy-naphthalen-1-yl)methylene]-5-(4-chlorophenyl)-1H-pyrazole-3-carbohydrazone (**7e**)*: Starting with **11f** and 2-hydroxy-1-naphthaldehyde, the same procedures were followed as in the synthesis of **1**. Yield = 48%; mp = 300–308 °C; ^{1}HNMR (400 MHz, DMSO-d_6) δ 13.95 (s, 1H), 12.93 (s, 1H), 12.19 (s, 1H), 9.69 (s, 1H), 8.17 (d, J = 8.4 Hz, 1H), 8.04 (d, J = 8.8 Hz, 1H), 7.94–7.89 (m, 4H), 7.63–7.57 (m, 3H), 7.41 (t, J = 7.6 Hz, 1H), 7.22 (t, J = 8.8 Hz, 1H); MALDI-MS m/z 391.1 $[M + H]^+$; HRMS (MALDI) m/z calcd $C_{21}H_{16}ClN_4O_2$ $[M + H]^+$ 391.0962, found 391.0958.

Biological assay

The ability of the compounds **1**–**7** to inhibit human recombinant DPP-4 was determined using a DPP-4 Drug Discovery Kit (Catalog No. BML-AK499, biomol) according to the manufacturer's instructions. A commercial DPP-4 Drug Discovery Kit (Biomol) was performed in 96-well flat-bottom plates in 100 μL reaction volume. The recombinant soluble human DPP-4 in 50 μL assay buffer (50 mM Tris, pH 7.5) was incubated for 15 min at room temperature with indicated concentrations of the compounds to be tested. Reactions were initiated by the addition of 50 μL of H-Gly-Pro-AMC (H-Gly-Pro-7-amino-4-methyl-

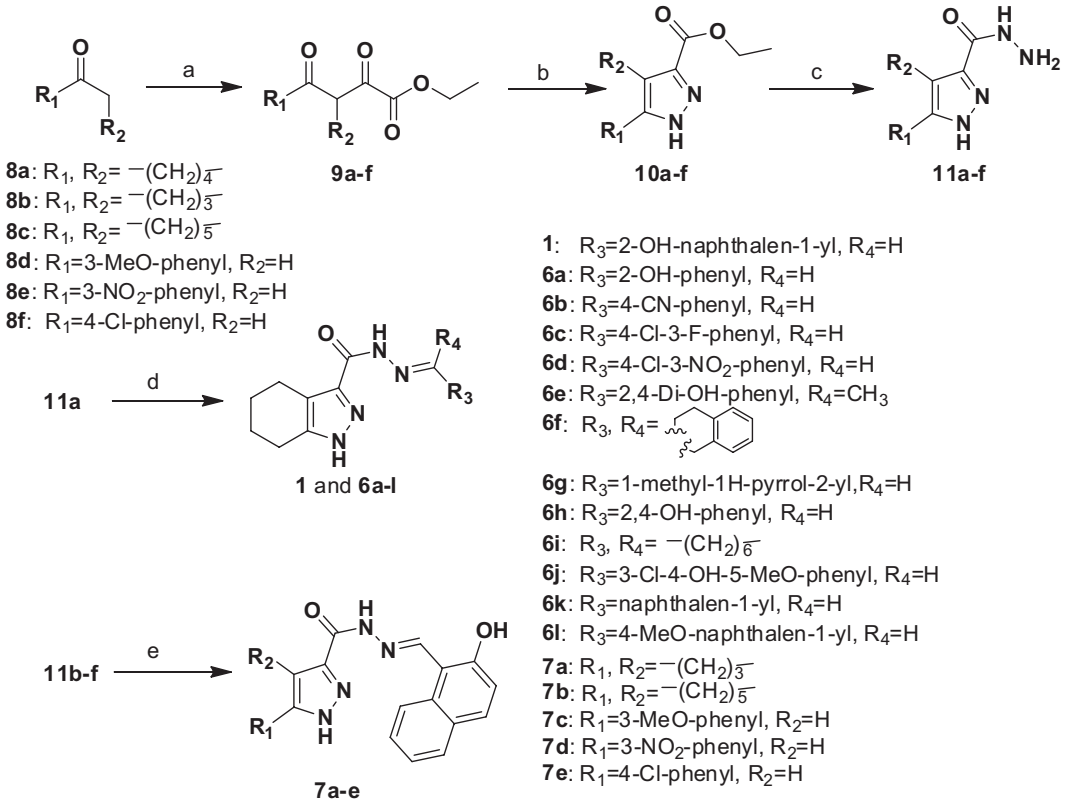

Scheme 1: Reagents: (a) Diethyl oxalate, CH_3CH_2ONa, 0 °C to room temperature, 6h; (b) NH_2–NH_2·H_2O, CH_3COOH, reflux, 8 h; (c) NH_2–NH_2·H_2O, CH_3CH_2OH, reflux, 8h; (d) R_3COR_4, CH_3COOH, reflux, 4 h; (e) 2-Hydroxy-1-naphthaldehyde, CH_3COOH, reflux, 4h.

coumarin, GPAMC) to a final concentration of 5 μM. Isoleucine thiazolidide (P32/98), a competitive transition-state substrate analog inhibitor of DPP-4, was used as a positive control (14), and DMSO (0.50% w/v) was used as a native control (NC). Compounds dilutions were prepared from stock in DMSO and diluted with assay buffer for inhibition assay. The increased fluorescence signal of 7-amino-4-methylcoumarin (AMC) (excitation at 380 nM and emission at 460 nM) was monitored for 20 min with 1-min interval using Synergy^{TM} 2 Multi-Mode Microplate Reader (BioTek, Winooski, Vermont, USA). The inhibitory rate (IR) was calculated by using the following equation.

$$IR(\%) = \left(1 - \frac{S_{compound}}{S_{NC}}\right) \times 100 \qquad (1)$$

where S represents slope that indicates the rate of reaction.

IC_{50} values were determined from the results of three independent experiments and calculated from the inhibition curves using the GraphPad Prism software (GraphPad Software Inc. La Jolla, CA, USA).

Results and Discussion

Analogue design and synthesis

Compound **1**-directed chemical modifications were performed in two cycles. First, we incorporated various steric, electronic, and hydrophobic groups at *N'*-positions of carbohydrazone in compound **1**, and twelve analogues (**6a**–**l**) were designed (Scheme 1) to determine whether 2-hydroxy-naphthalene moiety is necessary for inhibitor/DPP-4 interaction. Second, replacing cyclohexyl ring in compound **1** with rings of different sizes (cyclopentyl or cycloheptyl ring) and open-ring substituents, we synthesized five analogues (**7a**–**e**) (Scheme 1) to estimate whether the binding pocket of the DPP-4 around cyclohexyl ring has enough spatial volume available to accommodate large chemical moieties.

Scheme 1 depicts the sequence of reactions that led to the preparation of compounds **1**, **6a**–**l,** and **7a**–**e** using R_1, R_2-di-substituted ethanone (**8**) as the starting material. Treatment of **8** with diethyl oxalate and sodium ethoxide in anhydrous ethyl alcohol afforded α, γ-diketo ester **9**, followed by the twice condensation with hydrazine hydrate to obtain ethyl pyrazole-3-carboxylate **10** and carbohydrazide **11**, respectively. Finally, the condensation of compound **11** with different aldehydes or ketones giving the target compounds **1** and **6**–**7** (Table 1).

Biological activities and SARs

For the primary assay, using P32/98 (Isoleucine thiazolidide) as a positive control, the inhibition rates of the compounds **1**, **6a**–**l,** and **7a**–**e** at 10 μM were measured. The results are summarized in Table 1. Of the synthetic derivatives tested, nine compounds (e.g.,

Table 1: Chemical structures of compounds **1**, **6a**–**l**, **7a**–**e** and their activities

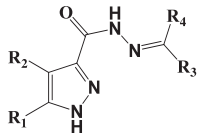

Compound	R_1	R_2	R_3	R_4	Inhibitory rate at 10 μM (%)	IC_{50} (μM)
1	–$(CH_2)_4$–		2-OH-naphthalen-1-yl	H	76.7	2.12
6a	–$(CH_2)_4$–		2-OH-phenyl	H	18.0	–
6b	–$(CH_2)_4$–		4-CN-phenyl	H	12.1	–
6c	–$(CH_2)_4$–		4-Cl-3-F-phenyl	H	19.6	–
6d	–$(CH_2)_4$–		4-Cl-3-NO_2-phenyl	H	2.5	–
6e	–$(CH_2)_4$–		2,4-Di-OH-phenyl	CH_3	24.1	70.80
6f	–$(CH_2)_4$–		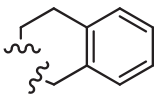		14.5	
6g	–$(CH_2)_4$–		1-methyl-1H-pyrrol-2-yl	H	31.9	52.48
6h	–$(CH_2)_4$–		2,4-Di-OH-phenyl	H	22.0	
6i	–$(CH_2)_4$–		-$(CH_2)_6$-		0	
6j	–$(CH_2)_4$–		3-Cl-4-OH-5-MeO-phenyl	H	3.4	
6k	–$(CH_2)_4$–		Naphthalen-1-yl	H	68.3	3.44
6l	–$(CH_2)_4$–		4-MeO-naphthalen-1-yl	H	52.8	18.20
7a	–$(CH_2)_3$–		2-OH-naphthalen-1-yl	H	38.2	43.65
7b	–$(CH_2)_5$–		2-OH-naphthalen-1-yl	H	53.0	19.50
7c	3-methoxyphenyl	H	2-OH-naphthalen-1-yl	H	47.9	16.59
7d	3-nitrophenyl	H	2-OH-naphthalen-1-yl	H	38.3	35.62
7e	4-chlorophenyl	H	2-OH-naphthalen-1-yl	H	42.3	18.61
P32/98					92.70	0.14

6e, **6g**, **6k–l,** and **7a–e**) displayed good inhibitory activities against DPP-4 (expressed as inhibitory rate at 10 μM ≥ 25%), indicating that these compounds were good candidate inhibitors of DPP-4. The half-maximal inhibitory concentration (IC_{50}) values, ranging from 2.12 to 70.80 μM (Table 1), were calculated by fitting the dose–response curve using the GraphPad Prism software with three independent determinations.

For further study on the DPP-4 selectivity for nine active compounds (**6e**, **6g**, **6k–l,** and **7a–e**), we calculated the ligand-receptor binding free energy for the active compounds with the three models of DPP-4, DPP-8, and DPP-9, respectively (Table S1, Supporting Information). According to the data listed in Table S1, we found that the values of the binding free energy of nine active compounds with the model of DPP-4 were all lower than the values of the binding free energy of them with the models of DPP-8 and DPP-9. These results indicated tentatively that our active compounds are DPP-4 selectivity over DPP-8 and DPP-9.

The SAR analysis of a set of eighteen compounds provided important insights into the essential structural requirements for effective DPP-4 inhibition. An analysis of the data shown in Table 1 revealed some noteworthy observations of the SAR for compounds **1, 6a–l,** and **7a–e**: (i) compared with non-naphthalene-containing compounds (**6a–d, 6f, 6h, 6i,** and **6j**), the naphthalene-containing analogs (**1**, **6k–l** and **7a-e**) all showed good activity (ranging from 2.12 to 43.65 μM), this means the naphthalene moiety was crucially important to the inhibitory activities; (ii) displacement of 2-OH substitution on naphthalene ring with 4-MeO (**1** versus **6l**) or removal of 2-OH substitution on naphthalene ring (**1** versus **6k**) substantially decreased the inhibitory activity of the derivatives, which implied the polar substituent has some contributions to the activity of the analogs; (iii) introduction of 4-MeO substitution on the naphthalene ring (**6k** versus **6l**) could not be tolerated, leading to a fivefold reduction in activity, which proposed that steric groups at 4-position of naphthalene ring were disadvantaged to the activity; (iv) replacement of the 2-OH-naphthalene ring with the 2,4-di-OH-phenyl (**1** versus **6e**) or the 1-methyl-pyrrolyl group (**1** versus **6g**) substantially decreases potency, which confirmed the significance of the naphthalene ring and the 2-OH substitution on it, respectively, and also suggested that the hydrophobic interaction was more important than the polar interaction (**6g** versus **6e**). (v) Among cyclohexane (**1**), cyclopentane (**7a**), cycloheptane (**7b**), and open-ring (**7c–e**) substituents, cyclohexane substituent was optimal, and significantly improved the biological activities (**1** versus **7a**, **1** versus **7b** and **1** versus **7c–e**).

Binding models

To address more information for SARs of the discovered DPP-4 inhibitors and to gain clues for further structural optimization, the binding models of the lead compound (**1**) and the two representative analogs (**6k** and **7c**) to DPP-4 were generated by using GLIDE 5.0.[d] Figure 2 showed the predicted binding poses of **1** (2A), **6k**

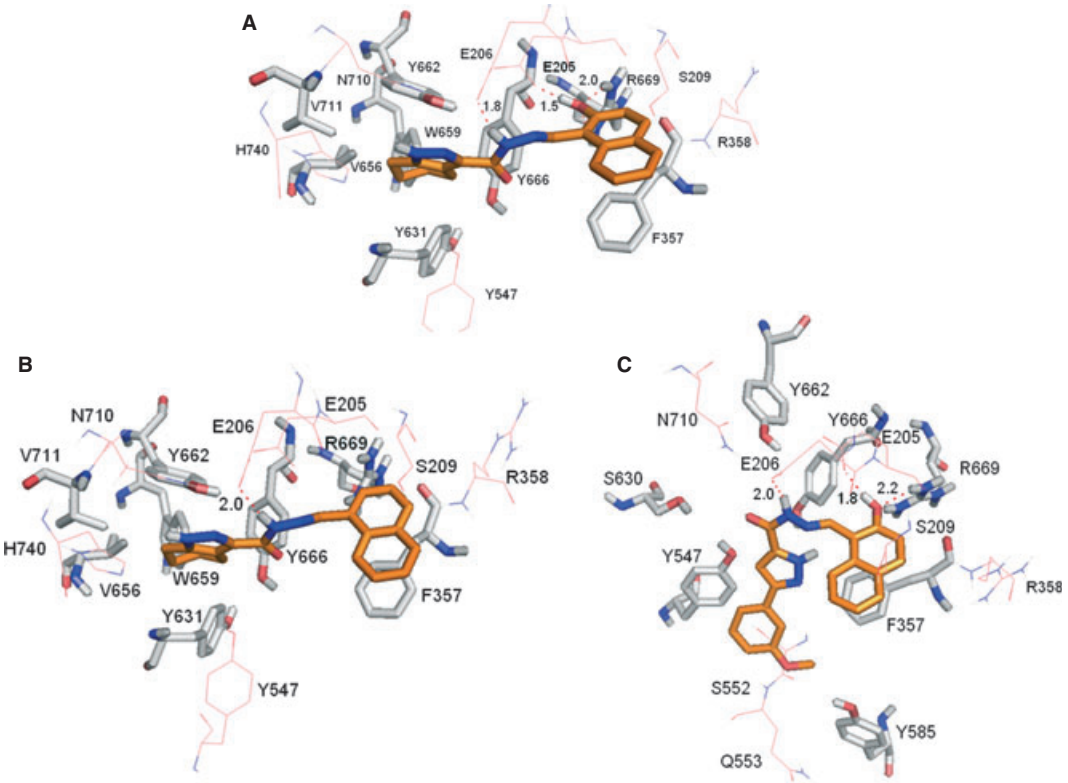

Figure 2: Three-dimensional (3D) interaction schemes of docked poses of **1** (A), **6k** (B), and **7c** (C) in the active sites of DPP-4. The ligands and critical residues of the binding pocket are shown as sticks, and the non-carbon atoms are colored by atom types (receptor carbon in gray and ligand carbon in orange). Hydrogen bonds are shown as dotted lines. All hydrogen atoms were not displayed.

(2B), and **7c** (2C) in the DPP-4 active site. It was obvious that the 4,5,6,7-tetrahydro-indazole moiety of compound **1** got tightly trapped in the hydrophobic cage formed by residues Tyr631, Val656, Trp659, Tyr662, Tyr666, Val711 (named as S1 pocket), and the α-amino group of carbohydrazone established the hydrogen bond interaction with the special residue Glu205 (Figure 2A). In addition, the 2-hydroxyl substitution on naphthalene ring formed hydrogen bond interactions with residues Glu206 and Arg669, and the naphthalene ring of compound **1** made the potent hydrophobic interaction with the residue Phe357, which was consistent with the result of dynamics performed by our group (15) (Figure 2A). For compound **6k**, its binding mode (Figure 2B) to DPP-4 was very similar to that of **1** to DPP-4, such as also forming hydrophobic interactions with the S1 pocket and the residue Phe357. These hydrophobic interactions play critical roles for maintaining the activity of analogs. Although compound **6k** was lack of 2-OH substitution on naphthalene ring, which led to the loss of the hydrogen bond interactions with residues Glu206 and Arg669 observed in the case of **1,** and was regarded as one of the key factors leading to ∼2 times potency decrease in compound **6k** compared with compound **1,** compound **6k** still exhibited the most potent inhibitory effect than other analogs. Unlike compounds **1** and **6k**, compound **7c** adopted a different docking conformation (Figure 2C); the 5-phenyl-pyrazole group deviated from the hydrophobic S1 pocket. The S1 pocket was spatially constrained and could not accommodate larger groups, especially polar groups, which caused the lower inhibitory activity of **7c**–**e** compared with **1**. All the experimental results were in agreement with the molecular-binding model.

Pharmacophore mapping

To further elaborate the SARs based on the ligand information, common feature pharmacophore models were generated by HipHop present in Catalyst 4.10[e] based on eight DPP-4 inhibitors (**1**-**5**, **6e**, **6k**, and **7d**, Table 2) and then top-ranking pharmacophore models were exported for further studies. As an internal validation of the pharmacophore models, the training set compounds were mapped onto the top four pharmacophore models. Based on the best-fit values and ΔE values of the training set compounds, hypo1 was chosen as the best pharmacophore model, which consisted of one HBD, one HBA, and two hydrophobic (HY) features (Figure 3). Our model hypo1 partially matched with the best pharmacophore model generated by HypoGen in 2008 (16), which further verified the accuracy of our model. Furthermore, the features of hypo1 were consistent with the 3D-QSAR model of DPP-4 inhibitors reported by our laboratory (17), which also proved our model was reasonable.

The 3D space and distance constraints of these pharmacophore features of hypo1 are shown in Figure 3A,B presented the hypo1 aligned with the most active compound **1**. It was revealed that the HBA matched 2-hydroxyl substitution on naphthalene ring; the hydrogen bond donor mapped with α-amino group of carbohydrazone; the two HY features mapped with cyclohexane ring of 4,5,6,7-tetrahydro-indazole moiety and benzene ring of naphthalene group, respectively. This pharmacophore mapping result was highly consistent with the docking result of the crystal structure of DPP-4. For example, the HBA and HBD features perfectly directed to the residues Arg669 and Glu205, respectively. One HY feature was close to the Phe357 and the other HY feature was corresponding to hydro-

Table 2: Structures and inhibitory activities of the training set compounds used to generate qualitative pharmacophore models

Compound	Structure	IC_{50} (μM)	Compoundd	Structure	IC_{50} (μM)
1	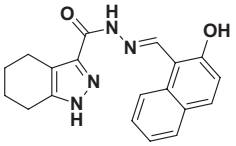	2.12	**5**	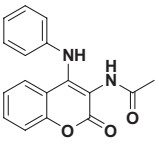	36.35
2	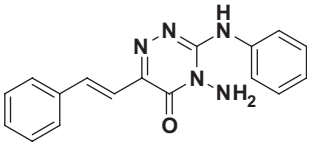	15.31	**6e**	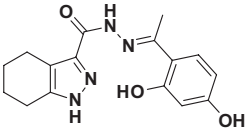	70.80
3	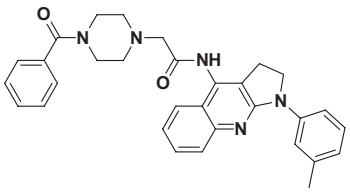	17.87	**6k**	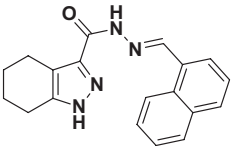	3.44
4	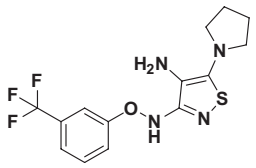	35.64	**7d**	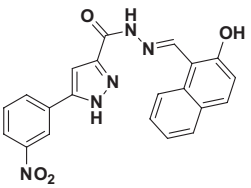	35.62

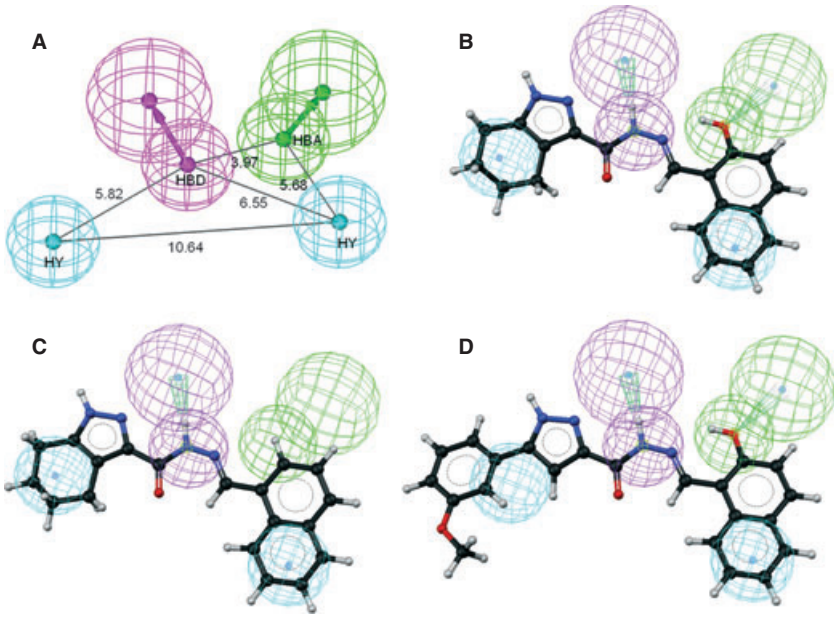

Figure 3: The best model Hypo1 (A) with distance constraints (in angstroms). Compound **1** (B), **6k** (C), and **7c** (D) mapped onto the pharmacophore model Hypo1. Pharmacophore features are color-coded with blue for HY, green for hydrogen bond acceptor, and purple for hydrogen bond donar.

phobic S1 pocket (Figure 2). The mapping results of the other active compounds were also encouraged and in accord with the docking results (Figure 3C–D). Compound **6k** missed the HBA feature of hypo1 so that it cannot form hydrogen bond interactions with the residues Glu206 and Arg669. For compound **7c**, one of the HY features was lost, which made it impossible to form the hydrophobic interaction with the S1 pocket. Pharmacophore mapping results were in good agreement with docking results. Besides, some guiding information was obtained for further structural optimization: based on the two key hydrophobic moieties (4,5,6,7-tetrahydro-indazole group and naphthalene ring), we may add some electric fragments to make interaction with surrounding polar residues, such as Glu205, Arg669, Asn710, His740 (Figure 2).

Conclusion

In summary, we have discovered novel inhibitors of DPP-4, featuring the pyrazole-3-carbohydrazone scaffold, using a structure-based virtual screening approach in conjunction with chemical synthesis and bioassay. Based on the structure of lead compound **1**, chemical modifications were performed in two cycles. Totally, seventeen new compounds have been synthesized and tested with biological assays. Finally, nine compounds (**6e**, **6g**, **6k**–**l,** and **7a**–**e**) were found to show micromolar or low-to-mid-micromolar level inhibitory effects against DPP-4. Molecular docking models give rational explanation about SARs. Based on eight DPP-4 inhibitors (**1**–**5**, **6e**, **6k**, and **7d**), the best pharmacophore model hypo1 was obtained, composed of one HBD, one HBA and two hydrophobic (HY) features. Both docking model and pharmacophore mapping results are in agreement with pharmacological results. The present studies give some guiding information for further structural optimization and are helpful for future inhibitors design.

Acknowledgments

We gratefully acknowledge the financial supports from the National Natural Science Foundation of China (Grants 21002028, 20902022 and 30973642), National S&T Major Project, China (Grant 2011ZX09102-005-02), the 111 Project (Grant B07023), the Fundamental Research Funds for the Central Universities, the Innovation Program of Shanghai Municipal Education Commission (Grant 10ZZ41), and the Shanghai Committee of Science and Technology (Grant 11DZ2260600).

References

1. Gorrell M.D., Gysbers V., McCaughan G.W. (2001) CD26: a multifunctional integral membrane and secreted protein of activated lymphocytes. Scand J Immunol;54:249–264.
2. Meester I.D., Durinx C., Proost P., Scharpe S., Lambier A.M. (2002) Ectopeptidases: CD13/Aminopeptidase N and CD26/Dipeptidylpeptidase IV in Medicine and Biology. New York: Kluwer Academic/Pleneu Publisher; pp. 223–257.
3. Mentlein R., Gallwitz B., Schmidt W.E. (1993) Dipeptidylpeptidase IV hydrolyses gastric inhibitory polypeptide, glucagon-like peptide-1 (7–36) amide, peptide histidine methionine and is responsible for their degradation in human serum. Eur J Biochem;214:829–835.

4. Kieffer T.J., McIntosh C.H., Pederson R.A. (1995) Degradation of glucose-dependent insulinotropic polypeptide and truncated glucagon-like peptide 1 in vitro and in vivo by dipeptidyl peptidase IV. Endocrinology;358:5–3596.
5. Kim D., Wang L.P., Beconi M., Eiermann G.J., Fisher M.H., He H.B., Hickey G.J. *et al.* (2005) (2R)-4-Oxo-4-[3-(trifluoromethyl)-5,6-dihydro[1,2,4]triazolo[4,3-α]pyrazin-7(8H)-yl]-1-(2,4,5-trifluorophenyl)butan-2-amine: a potent, orally active dipeptidyl peptidase IV inhibitor for the treatment of type 2 diabetes. J Med Chem;48:141–151.
6. Villhauer E.B., Brinkman J.A., Naderi G.B., Burkey B.F., Dunning B.E., Prasad K., Mangold B.L., Russell M.E., Hughes T.E. (2003) 1-[[(3-hydroxy-1-adamantyl)amino] acetyl]-2-cyano-(S)-pyrrolidine: a potent, selective, and orally bioavailable dipeptidyl peptidase IV inhibitor with antihyperglycemic properties. J Med Chem;46:2774–2789.
7. Augeri D.J., Robl J.A., Betebenner D.A., Magnin D.R., Khanna A., Robertson J.G., Wang A.Y. *et al.* (2005) Discovery and preclinical profile of saxagliptin (BMS-477118): a highly potent, long-acting, orally active dipeptidyl peptidase IV inhibitor for the treatment of type 2 diabetes. J Med Chem;48:5025–5037.
8. Feng J., Zhang Z., Wallace M.B., Stafford J.A., Kaldor S.W., Kassel D.B., Navre M., Shi L., Skene R.J., Asakawa T., Takeuchi K., Xu R., Webb D.R., Gwaltney S.L. (2007) Discovery of alogliptin: a potent, selective, bioavailable, and efficacious inhibitor of dipeptidyl peptidase IV. J Med Chem;50:2297–2300.
9. Eckhardt M., Langkop E., Mark M., Tadayyon M., Thomas L., Nar H., Pfrengle W., Guth B., Lotz R., Sieger P., Fuchs H., Himmelsbach F. (2007) 8-(3-(R)-aminopiperidin-1-yl)-7-but-2-ynyl-3-methyl-1-(4-methyl-quinazolin-2-ylmethyl)-3,7-dihydropurine-2,6-dione (BI 1356), a highly potent, selective, long-acting, and orally bioavailable DPP-4 inhibitor for the treatment of type 2 diabetes. J Med Chem;50:6450–6453.
10. Biftu T., Scapin G., Singh S., Feng D., Becker J.W., Eiermann G., He H. *et al.* (2007) Rational design of a novel, potent, and orally bioavailable cyclohexylamine DPP-4 inhibitor by application of molecular modeling and X-ray crystallography of sitagliptin. Bioorg Med Chem Lett;17:3384–3387.
11. Snyder H.R., Brooks L.A., Shapiro S.H. (1943) Pimelic acid. Org Synth;2:531.
12. van Herk T., Brussee J., van den Nieuwendijk A.M.C.H., van der Klein P.A.M., IJzerman A.P., Stannek C., Burmeister A., Lorenzen A. (2003) Pyrazole derivatives as partial agonists for the nicotinic acid receptor. J Med Chem;46:3945–3951.
13. Kirchner F.K., Bethlehem N.Y. (1961) 1-(3-Indazolecarbonyl)-hydrazines and their preparation. Patent No. US3007938.
14. Demuth H.U., McIntosh C.H., Pederson R.A. (2005) Type 2 diabetes-therapy with dipeptidyl peptidase IV inhibitors. Biochim Biophys Acta;1751:33–44.
15. Li C., Shen J., Li W.H., Lu C.H., Liu G.X., Tang Y. (2011) Possible ligand release pathway of dipeptidyl peptidase IV investigated by molecular dynamics simulations. Proteins;79:1800–1809.
16. Lu I.L., Tsai K.C., Chiang Y.K., Jiaang W.T., Wu S.H., Mahindroo N., Chien C.H., Lee S.J., Che X., Chao Y.S., Wu S.Y. (2008) A three-dimensional pharmacophore model for dipeptidyl peptidase IV inhibitors. Eur J Med Chem;43:1603–1611.
17. Zeng J., Liu G.X., Tang Y., Jiang H.L. (2007) 3D-QSAR studies on fluoropyrrolidine amides as dipeptidyl peptidase IV inhibitors by CoMFA and CoMSIA. J Mol Model;13:993–1000.

Notes

[a]http://www.cdc.gov/Features/Livingwithdiabetes/.
[b]World Health Organization at http://www.who.int/diabetes/facts/world_figures/en/.
[c]http://www.diabetesatlas.org/.
[d]GLIDE version 5.0. New York, NY: Schrödinger, LLC; 2009. http://www.schrodinger.com/.
[e]LIGPREP version 2.2. New York, NY: Schrödinger, LLC; 2005. http://www.schrodinger.com/.
[f]CATALYST User Guide, Version 4.10 (Software Package). San Diego, CA, USA: Accelrys Inc. http://accelrys.com/.

Supporting Information

Additional Supporting Information may be found in the online version of this article:

Table S1. The predicted binding free energies of the active compounds (**1**, **6e**, **6g**, **6k**–**l**, and **7a**–**e**) with the receptors (DPP-4, DPP-8 and DPP-9) by MM-GBSA method.

Please note: Wiley-Blackwell is not responsible for the content or functionality of any supporting materials supplied by the authors. Any queries (other than missing material) should be directed to the corresponding author for the article.